Chapter 4

Numerical Experiments

4.1 Error estimators and adaptive refinement

Due to singularities the convergence of finite element solutions on uniform grids can be arbitrarily low. Adaptivity based on a-posteriori error estimators overcomes this problem. It may lead to convergence rates (measured in terms of nodes) as in the regular case without singularities. Results in this chapter report the performance of the derived error estimators applied to various problems. We include calculations done with 2D model problems and real data as well as with 3D model problems.
Let us first discuss how to judge the performance of a-posteriori error estimators. A proper criterion for the quality of the error estimator is the reduction of the error in the course of refinement based on the estimator. As we are using piecewise linear Finite Elements we expect a convergence rate of $N^{-1/d}$, where N is the number of nodes. For calculating the error one has to know the exact solution or one can get an approximation calculating a so-called reference solution on a mesh that is much finer than the adaptive. In the same way the estimated error should be reduced with the expected optimal order $O(N^{-1/d})$ in the course of the refinement. A decrease worse than $O(N^{-1/d})$ indicates an efficiency index not of order $O(1)$ or a non-optimal refinement strategy. In contrast to the error reduction of order $O(N^{-1/d})$ for adapted meshes the reduction of the error on uniform grids will in general be not better than $O(N^{-\lambda/d})$, if the solution u has piecewise $H^{1+\lambda}$-regularity only. To see this in the 2D-case we refer to remark 3.1. In the 3D-case extend the function mentioned in remark 3.1 constantly in z-direction. For a discussion about 3D edge singularities see section 4.7.3.
An important reason of using error estimators is the wish to control the error. Hence a criterion for judging an estimator is the efficiency index, that is the ratio

$$\tau := \eta / \ |u - u_h|_{kH^1(\Omega)}$$

which should be close to 1 or constant and problem independent.
From theory one can explicitly calculate the factors in the upper and lower bound of the efficiency index. They depend only on the shape regularity of the family of triangulations $\{\mathcal{T}_h\}$. However, these bounds may be to pessimistic. Doing calculations on a large class of problems one can check constants for the lower bound τ_{inf} and upper bound τ_{sup} of the efficiency index. Rescaling with $1/\tau_{inf}$ an efficiency index greater than the

error can be assured (at least for the range of the problems considered). We want to mention that throughout the following numerical experiments we did no scaling of the error estimators at all.
It would be desirable that $\tau_{inf} = \tau_{sup} = 1$ but this is not covered by the present theory. For recent developments to overcome this difficulty see [3] [42].
However, it may happen that the efficiency index tends asymptotically to a *problem independent constant*. This was observed in our numerical experiments for model problems independent of their regularity. Rescaling with this constant the estimator can be improved. Obviously, the solutions used in numerical examples should have typical properties of solutions of interface problems such as singularities.
It is known that the error reduction for regular solutions (that means piecewise contained in H^2) is of optimal order already for uniform refinement. Nevertheless, adaptive refinement for regular solutions can lead to lower errors than uniform refinement. Such behaviour can be explained as follows. Suppose, that on the coarse mesh, the error is not equally distributed. Refining parts of the domain with large errors, the error will be reduced noticeable, whereas the number of nodes does not increase much.

4.2 Implementation issues

The whole code is written within the software package `pdelib`, which is developed at the Weierstrass Institute of Applied Mathematics and Stochastics (see `http://www.wias-berlin.de/~pdelib/index.html`) [27]. This package supports the idea of programming in a dimension-less manner. In such a way the error estimators are implemented. Thus they work in 2D as well as on 3D grids.
The idea of the refinement procedure is to refine simplices with large error estimators η_T. The first work dealing with error reduction rates [22] states that after reducing in a pre-refinement step the data oscillation $\|f - f_h\|_{L^2(T)}$, the error will be reduced with geometrical order by realizing the marking strategy described below. This approach has been extended to the case of varying coefficients under some regularity assumptions [21]. For the Laplace equation it has been shown that reduction of data oscillation and of the error estimators can be done simultaneously [41] [42]. As the right hand side f vanishes in our numerical examples, data oscillation vanishes too.
We now describe the marking strategy following [22]. First we calculate the estimators. We mark simplices for refinement where the estimator takes on the largest values until the sum of the squares of the estimators on marked simplices reaches a certain threshold θ (for instance $\theta = 20\% = 0.2$) of the square of the estimated global error.
The following pseudo-code is used to realize the marking strategy [22]). Given local estimators η_T and given $\theta \in [0, 1]$ and $0 < \nu << 1$, for instance $\theta = 0.2, \nu \in \{0.01, 0.1\}$, perform

η_{max}`:=`$\max(\eta_T; T \in \mathcal{T}_h)$
`sum:=0`
$\gamma := 1$
`while sum` $\leq \theta\ \eta^2$
  γ `:=` $\gamma - \nu$

```
  for all T ∈ T_h
    if T is not marked
      if η_T > γ η_max
        mark T for refinement
        sum := sum + η_T^2
      end if
    end if
  end for
end while
```

If $\theta = 1.0$, refinement will be uniform and if $\theta = 0.0$, no simplex will be refined.
Marked simplices will be refined by the adaptive kernel of the program `kaskade` from Konrad-Zuse-Zentrum für Informationstechnik Berlin (`http://www.zib.de/`)[10] which is called through to the grid interface of `pdelib`. The refinement is of red type where a green closure [57] is applied. That means in 2D refined triangles are divided into four equal triangles and if necessary neighbouring triangles are bisected. When a part of a bisected triangle has to be refined, bisection is revoked and the triangle will be divided into four similar ones. In this way degeneration of simplices in the course of refinement will be prevented.
Although for model problems the solution u is known we have to apply quadrature rules to approximate $|u - u_h|_{kH^1(\Omega)}$. We approximate $|u - u_h|_{kH^1(\Omega)}$ by $\widehat{\eta} := |u_Q - u_h|_{kH^1(\Omega)}$ where u_Q is a piecewise quadratic interpolation of u on a reference mesh. To capture the behaviour of the singularity one has to take care to construct an reference mesh which is fine enough.
The reference grid has been constructed as follows: Each adaptive mesh is 4 times globally refined. To those simplices with the singular point as a node we apply recursive refinement up to a final minimum mesh width of $1e-80$. As the singular point was situated at the origin the mesh was refined only there. In such a way grids with such a small mesh width can be represented with double-precision arithmetic.
Simulations with reference meshes which were coarser or finer than the one described above, indicated the reliability of the obtained results. For piecewise regularity greater than say $H^{1.2}$ one can rely on less refined reference meshes, but in case of deteriorating regularity very fine reference meshes are indeed necessary.

4.3 Error reduction rates for an example with $H^{1+3/4}$ regularity

The solution of our model problem will be the singular function defined in example 2.1 from section 2.4.3. Dirichlet boundary conditions are given by the singular function. We use the error estimators η_R, η_D and η_H which are defined in section 3.6.
In figures 4.1 and 4.2 we plot an adapted mesh for the case $k_2 \in \{0.01, 100\}$. The initial mesh is based on a 4×4 tensor grid with 16 squares, each subdivided into two triangles in the same way. In case $k_2 = 100$ we have $u \notin H^2(\Omega_i), i = 1, 2$, and the refinement takes place mainly near the singularity. In the case $k_2 = 0.01$ it yields $u \in H^2(\Omega_i), i = 1, 2$, and the refinement proceeds in the whole domain (although the mesh is finer in the neighbourhood of the origin).

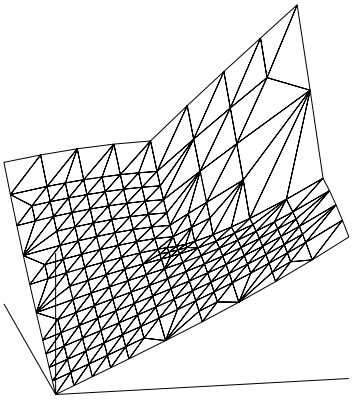

Figure 4.1: $k_2 = 0.01$, refined mesh for a regular solution $u \in H^2(\Omega_i)$, refinement in large areas

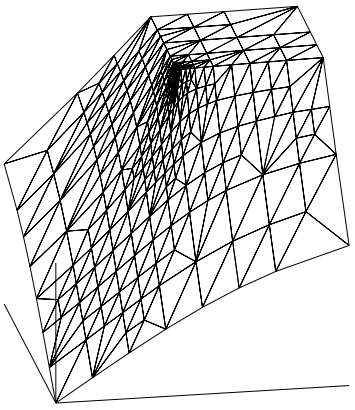

Figure 4.2: $k_2 = 100$, refined mesh for a non-regular solution $u \notin H^2(\Omega_i)$, refinement takes place at the singularity

In Figure 4.3 we plot the reduction of the error over the number of nodes for three different estimators for $k_2 = 100$. Our results show that all estimators reduce the error

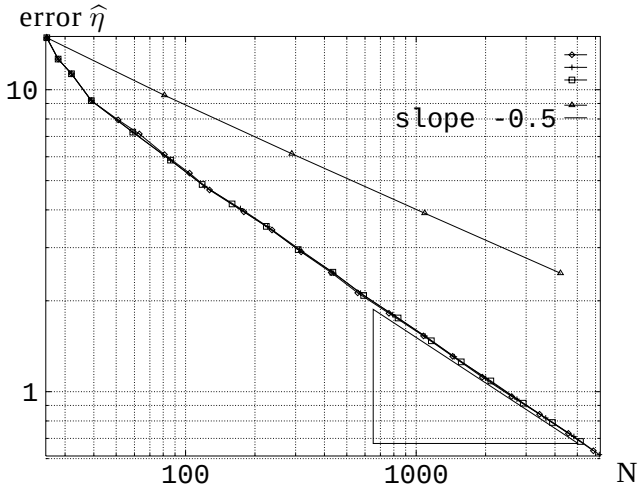

Figure 4.3: $k_2 = 100$, solution $u \notin H^2(\Omega_i)$, optimal reduction of the error for refinement with $\eta_R(\diamond), \eta_H(+), \eta_D(\square)$ and non-optimal reduction for uniform$(\triangle)$ refinement; triangle has slope -0.5

equally well and at least with the optimal convergence rate $O(N^{-1/2})$. The depicted triangle has a slope of $-1/2$. For comparison we have plotted also the reduction of the error in the course of uniform refinement. Here one clearly sees the advantage of the adaptive procedure. The same error is achieved on an adaptively refined mesh with 180 unknowns and a uniformly refined mesh with 1000 unknowns.

Qualitatively the same results are obtained in the case $k_2 = 0.01$ (see Figure 4.4). Remember that in this case u belongs to $H^2(\Omega_i)$. Again the depicted triangle has a

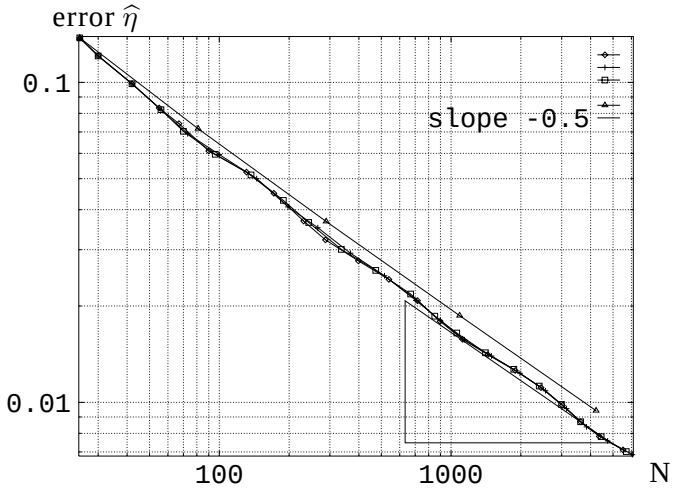

Figure 4.4: $k_2 = 0.01$, solution $u \in H^2(\Omega_i)$, optimal reduction of the error for refinement with $\eta_R(\diamond), \eta_H(+), \eta_D(\square)$ and uniform$(\triangle)$ refinement, triangle has slope -0.5

slope of exactly $-1/2$. Thus we have a convergence rate note worse than $O(N^{-1/2})$. The uniform refinement reduces the error with an order not higher as the estimators do. There is only little advantage of the refinement based on the estimators. The same error is achieved on an adaptively refined mesh with 850 and an uniformly refined mesh with approximately 1050 unknowns. It seems that adaptive refinement will be ahead also asymptotically.
The efficiency indices are plotted in figures 4.5 together with the efficiency index obtained for other values of k_2. We see that the efficiency index decreases moderately over the number of unknowns by a factor of at most 1.5. For a discussion of the efficiency index see the next section.

4.4 Robustness for an example with $H^{1+3/4}$ regularity

The problem setting is as in example 2.1 in section 2.4.3. To confirm theoretically proved robustness we carried out numerical experiments with $k_2 \in \{10^{-5}, 10^{-3}, 10^{-1}, 10^{1}, 10^{3}, 10^{5}\}$. We observed for all values k_2 and for all estimators η_R, η_D, η_H a reduction of the error with order $O(N^{-1/2})$. As depicted in Figure 4.5, the efficiency index for η_R is not constant but there is only a moderate dependency on k_2 and the number of nodes. The efficiency index takes on values between 2.6 and 3.8. It seems that for the irregular case, that is for $1 < k_2$ and $u \notin H^2(\Omega_i)$, it has larger variations than in the regular case $k_2 < 1$. Note that asymptotically it takes on the same value independent of the parameter k_2.
For the estimators η_D and η_H the efficiency indices take on also asymptotically the same values independent of the parameter k_2.

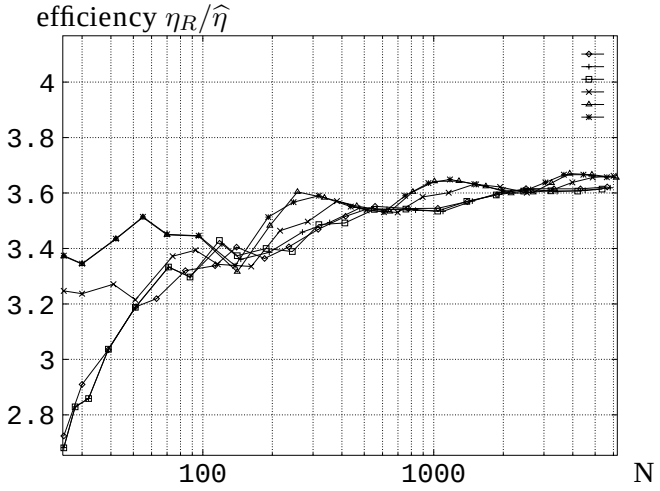

Figure 4.5: Efficiency indices for η_R and $k_2 \in \left\{10^1(\diamond), 10^3(+), 10^5(\square),\ 10^{-1}(\times), 10^{-3}(\triangle), 10^{-5}\right\}$

4.5 Examples with deteriorating regularity

The continuous problem is chosen in such a way that the solution is the singular function from example 2.2 from section 2.4.3. Dirichlet boundary conditions are given by the singular function. An adapted mesh is depicted in Figure 4.6. We see strong refinement around the singular point.

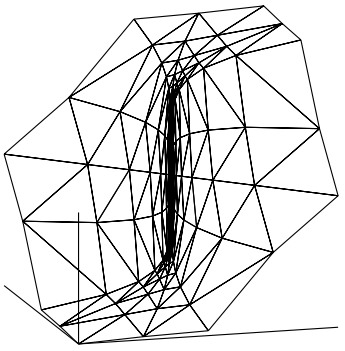

Figure 4.6: $u \notin H^{1+0.1}(\Omega_i)$, strong refinement around the singularity

Let us first present results obtained on uniform meshes. The regularity of u drops down if λ decreases. With decreasing regularity also the convergence rate on uniform meshes will be smaller, see remark 3.1. This is confirmed through calculations done on uniform and subsequently globally refined, uniform meshes for different values of $\lambda \in \{0.4, 0.2, 0.1, 0.05\}$

theory λ	numerics μ
0.4	0.405
0.2	0.22
0.1	0.15
0.05	0.12

Figure 4.7: Theoretically predicted λ versus observed convergence rate μ of $\widehat{\eta}$

In the Table 4.7 we compare the convergence rate μ of the reference error $\widehat{\eta}$ obtained between the last two refinement levels with approximately 4000 and 16000 unknowns with the predicted asymptotical convergence rate λ. We see that μ is greater than λ, but we may expect that μ decreases further for subsequent refinement levels.

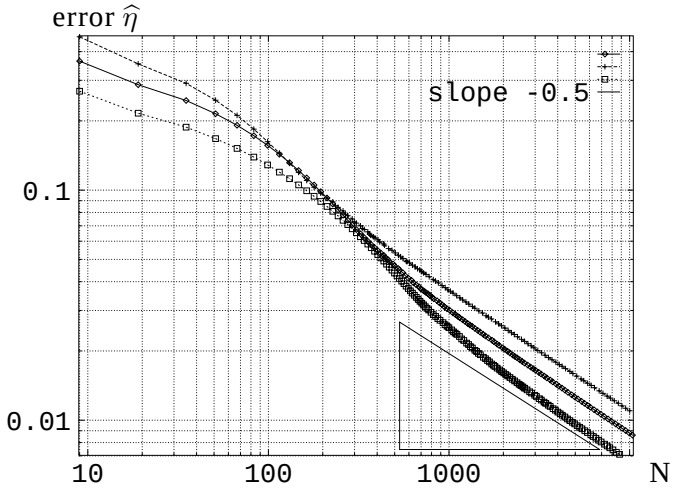

Figure 4.8: Error reduction for $\lambda \in \{\ 0.2(+),\ 0.1(\diamond),\ 0.05(\square)\ \}$ with order $O(N^{-1/2})$, triangle has slope -1/2, refinement on the basis of estimator η_R

Note that in this example the diffusion coefficients k_T are not quasi-monotonically distributed around the singular point. Recall that in this case we were not able to prove robust reliability for the error estimator. That means that the error can be underestimated if λ goes to 0. The resulting meshes may in turn lead to a non-optimal reduction of the error. The reference error is calculated as before.
In Figure 4.8 we plot the reduction of $\widehat{\eta}$ over the number of unknowns in the course of adaptive refinement. The approximation of the error $\widehat{\eta}$ is reduced with optimal order $O(N^{-1/2})$ for $\lambda = 0.2, 0.1, 0.05$. Here we marked only those simplices whose estimated error made up $\theta = 2\% = 0.02$ of the global error.
In Figure 4.9 the approximated efficiency index is plotted. One sees that the approximated efficiency index becomes smaller for smaller λ but nevertheless approximately the same asymptotical value 3.6 is reached as in subsection 4.4. A closer look onto the refinement history reveals that the prominent kink at 211 nodes for $\lambda = 0.2$ coincides with the first refinement of a simplex which has no node on the singularity. The same

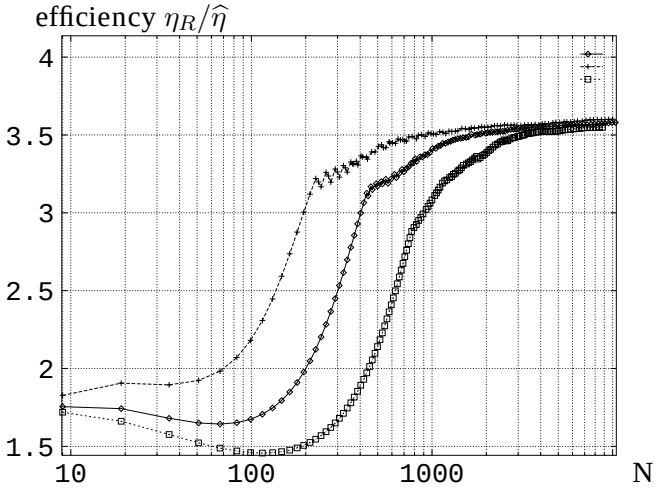

Figure 4.9: Efficiency index for adaptive refinement, $\lambda \in \{\ 0.2(+),\ 0.1(\diamond),\ 0.05(\square)\ \}$ decreases with decreasing λ, refinement on the basis of estimator η_R

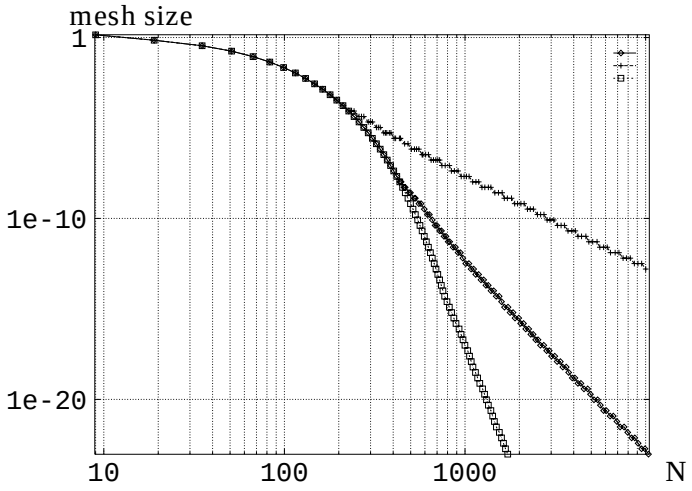

Figure 4.10: Minimum mesh size for $\lambda \in \{\ 0.2(+),\ 0.1(\diamond),\ 0.05(\square)\ \}$, minimum mesh size decreases with decreasing λ, refinement on the basis of estimator η_R

is true for $\lambda = 0.1$ and 435 nodes and $\lambda = 0.05$ and 771 nodes. We may say that at these stages the singularity is resolved.

We notice that the efficiency index as a function of the number of nodes is not anymore a monotone function as it was in the quasi-monotone case. We observe a local minimum that takes on lower values as the regularity decreases. Although the efficiency indices takes on moderate values from the interval [1.4,3.7] we do not know how they will evolve for lower regularity than $H^{1.05}$-regularity.

The refinement level where for the first time a simplex outside the singularity is refined, is seen also on the next Figure 4.10 where the minimum mesh size is plotted. One sees that the smaller the λ the more the mesh is refined. For $\lambda = 0.1$ and 650 unknowns the

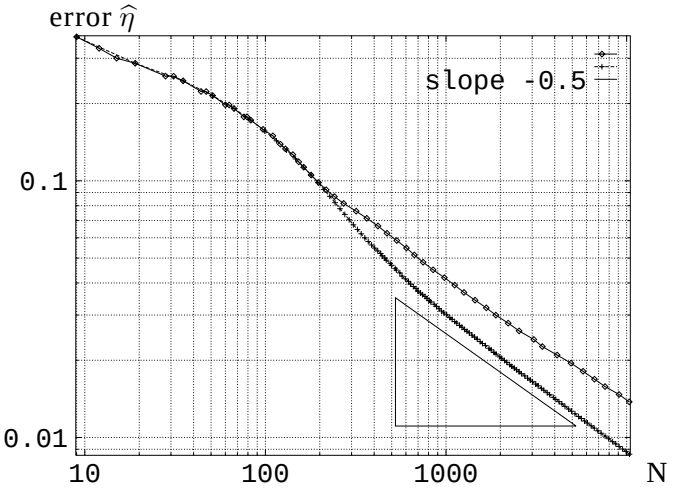

Figure 4.11: Different error reduction for $\theta = 0.2(\diamond), \theta = 0.02(+)$, $\lambda = 0.1$, error reduction with order $O(N^{-1/2})$ in case $\theta = 0.02$, triangle has slope -1/2, refinement on the basis of estimator η_R

minimum mesh-size is $1e-10$. For the case $\lambda = 0.05$ with 9500 nodes we reached a minimum mesh-size of $1e-39$.
If the solution u is obtained in the context of a physical model the validity of the model could be exceeded by calculating on such fine meshes.
Experiments where $\theta = 20\% = 0.2$ of the error were refined have led to less refined grids on which the error was reduced to a lesser extent when compared with the adaptive strategy where $\theta = 0.02$ (Figure 4.11).
Note that in the case $\theta = 0.2$ the efficiency index has not achieved that asymptotic value 3.6, Figure 4.12. We conclude that the experiments indicate non-robustness of the derived error estimators in the case of deteriorating regularity. In the next section we will further investigate this topic.
We want to mention that qualitatively the same results have been observed in the case of a refinement procedure that started from an initial grid which was pre-refined near the boundary. In such a way we can exclude possible additional errors caused by approximation of non-homogeneous boundary conditions.

The local efficiency index for deteriorating problems

For non quasi-monotonous diffusion coefficients with large variations we were not able to bound the local error by the error estimators in a robust way. We do not know if this is only a technical difficulty. In this section we will further investigate why the error estimators fails to generate, in our adaptive procedure, efficient grids in case of $\theta = 0.2$.
As in the previous section we choose $u := \psi_2$ defined in example 2.2 as the solution of a model problem. Recall that the singular point is located at the origin. Let us first make the following observations.

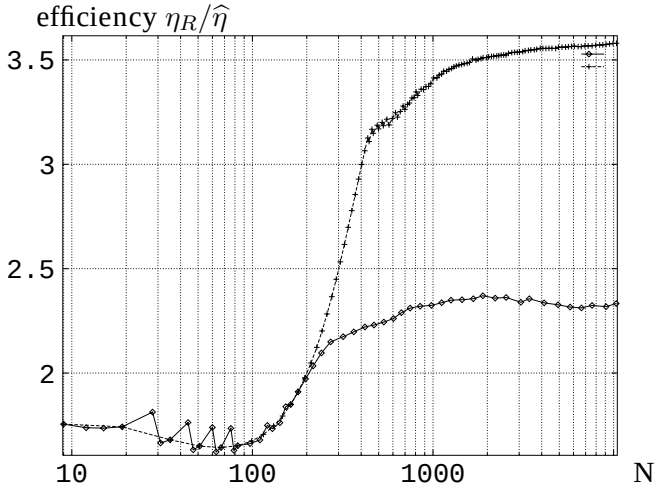

Figure 4.12: Efficiency index for adaptive refinement with $\theta = 0.2(\diamond), \theta = 0.02(+)$, $\lambda = 0.1$, refinement on the basis of estimator η_R

Remark 4.1 *Calculation shows that*

$$|u|_{kH^1(B_0(h))} \approx h^\lambda \quad ,$$

where $B_0(h)$ is the ball with center at the singularity and radius h. Denote by h_λ the radius of the ball $B_0(h_\lambda)$ where 50% of the global energy norm are attained. We calculate that $h_\lambda \approx 0.5^{1/\lambda} \approx 1e-3$ if $\lambda = 0.1$ and $h_\lambda \approx 1e-6$ (!) for $\lambda = 0.05$. That means that the solution u has a highly non-uniform behaviour.

We define the discrete neighbourhood of the origin

$$\omega_0 := \bigcup_{T \ni (0,0), T \in \mathcal{T}_h} T \text{ and } \eta^2_{R,0} := \sum_{T \subset \omega_0} \eta^2_{R,T}$$

the contributions of the local error estimators next to the origin.
The *local efficiency index* is defined as

$$\tau_0 := \frac{\eta_{R,0}}{|u - u_h|_{kH^1(\omega_0)}} \quad .$$

In this section we use a initial grid which is refined near the boundary in order to reduce a possible error caused by approximation of non-homogeneous boundary conditions. On each side of the domain there are located approximately 100 equidistant nodes. The initial grid has about 1900 nodes. We stop the adaptive procedure with a adapted mesh with approx. 10000 nodes.
In Figure 4.13 we plot the efficiency index τ and the local efficiency index τ_0 for $\lambda \in \{0.8, 0.4, 0.2, 0.1, 0.05\}$ and $\theta = 0.01$. In the course of refinement both τ and τ_0 tend to constant asymptotic values, which we denote by τ_∞ and $\tau_{0,\infty}$.
Comparing these values we see firstly that $\tau_{0,\infty}$ is smaller than τ_∞ and secondly that asymptotically $\tau_{0,\infty}$ depends on λ whereas τ_∞ is asymptotically independent of λ. In

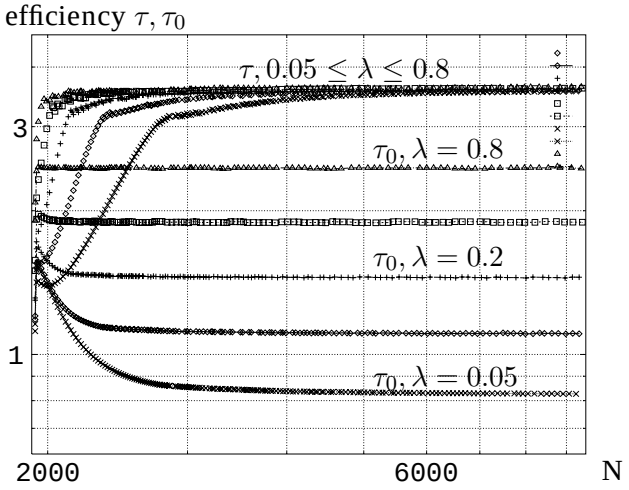

Figure 4.13: Efficiency index τ (points) and τ_0 (lines with points) for η_R and $\lambda \in \{\ 0.8(\triangle+),\ 0.4(\square),\ 0.2(+),\ 0.1(\diamond),\ 0.05(\times)\ \}$, τ_∞ independent of λ, $\tau_{0,\infty}$ decreases with decreasing λ

other words, the local error in the discrete neighbourhood ω_0 is really underestimated by the error estimator and the ratio between $\tau_{0,\infty}$ and τ_∞ becomes smaller as $\lambda \to 0$. A closer look on the dependence of the asymptotic value of the local efficiency index $\tau_{0,\infty}$ reveals a behaviour like $\tau_{0,\infty} \approx c\lambda^\beta$, see the table in Figure 4.14. We calculate $c \approx 2.678, \beta \approx 0.38$.

$\tau_{0,\infty}$	$2.68 \cdot \lambda^{0.38}$
2.46	2.46
1.89	1.89
1.45	1.45
1.11	1.12
0.83	0.86

Figure 4.14: Exponential dependence of $\tau_{0,\infty}$ from λ

Implications for the error estimator

On the basis of remark 4.1 we conclude that, in order to equidistribute the error, the finite element meshes should have simplices contained in the neighbourhood $B_0(h_\lambda)$ of the origin. Having in mind the low approximation order of Finite Elements for problems with low regularity we see that the simplices contained in the ball $B_0(h_\lambda)$ should be additionally strongly refined. We may then expect that for small λ an optimal refinement strategy consists in subsequent refinement of the simplices which have the origin as a node as long as the approximation error on the ball $B_0(h_\lambda)$ is not small enough.
Underestimation of the local error influences the global efficiency index. This influence becomes especially critical when the global error depends mainly on the local error

$|u - u_h|_{kH^1(\omega_0)}$, as we may expect. The effect of the underestimation of the local error vanishes if the singularity is sufficently fine resolved.
The dependence of the adapted grids from the parameter θ is explained in the same way. We know that the error estimator does not reflect the behaviour of the error, as can be seen from the numerical experiment from section 4.5. Nevertheless, the error estimators $\eta_{R,T}$ attains its maximum in ω_0. With the strategy where $\theta = 0.02$ (section 4.5) we marked in fact only those simplices with the *maximum estimated error* $\eta_{R,T}$ and that's why we came to efficient grids. Choosing $\theta = 0.2$ "too much" simplices away from the singularity were refined what led to an insufficient resolution of the singularity and hence to inefficient grids.

4.6 Examples with real data

In this section we will test the error estimators on more complicated geometries and data. This data comes from groundwater flow simulation problems considered by the WASY GmbH (`http://www.wasy.de`). In a soil saturated with water the flow of the water is ruled by a diffusive law, called Darcy's law. In this manner the solution of the respective elliptic problem can be seen as the pressure of the water (after addition of the pressure term caused by gravitation) and is known as hydraulic head. The gradient of the solution multiplied by the diffusion is a measure of the flux of the water. The transmissivity of the soil with respect to the water (that means the diffusion) differs for different types of soil. For instance the transmissivity of clay is by a factor of at least $1.e6$ smaller than that of sand.

4.6.1 Reliability of the reference error

For complicated real problems there are no analytical solutions known. To judge the quality of the estimated error we have to calculate a sufficiently good approximation $u_{ref,m}$ of the solution of the continuous problem on a reference mesh. We then use $\widehat{\eta}_m = |u_{ref,m} - u_h|_{kH^1(\Omega)}$ as the reference error. The reference mesh is constructed by m times globally refining the finest mesh obtained in the refinement cycle.
Clearly the reference error will depend on m. In a first experiment we discuss the reliability of the reference errors $\widehat{\eta}_m$ in an example where the analytical solution is known. Here we take the setting from example 2.2 with $k_2 = 100$. In Figure 4.15 we compare the reference errors for different values of $m = 1, 2, 3$. Additionally we plot the error obtained from the known analytical solution which is interpolated on a one time globally refined grid with P2 elements.
Figure 4.15 a) shows that the error is underestimated by $\widehat{\eta}_1, \widehat{\eta}_2, \widehat{\eta}_3$ and the smaller the index m the larger the underestimation. Further for a constant index m the underestimation of $\widehat{\eta}$ by $\widehat{\eta}_m$ is smaller at lower refinement levels.
The approximation $\widehat{\eta}_1$ leads to the worst approximation of the error and one notices an underestimation of at most 20% for a larger number of nodes.
In Figure 4.15 b) we depict the according efficiency indices, that is the ratios $\eta_R/\widehat{\eta}_m$.
As the error is underestimated by $\widehat{\eta}_m$ we observe a higher approximated efficiency index $\eta_R/\widehat{\eta}_m$ for lower values of m and higher numbers of nodes. Doing in the following

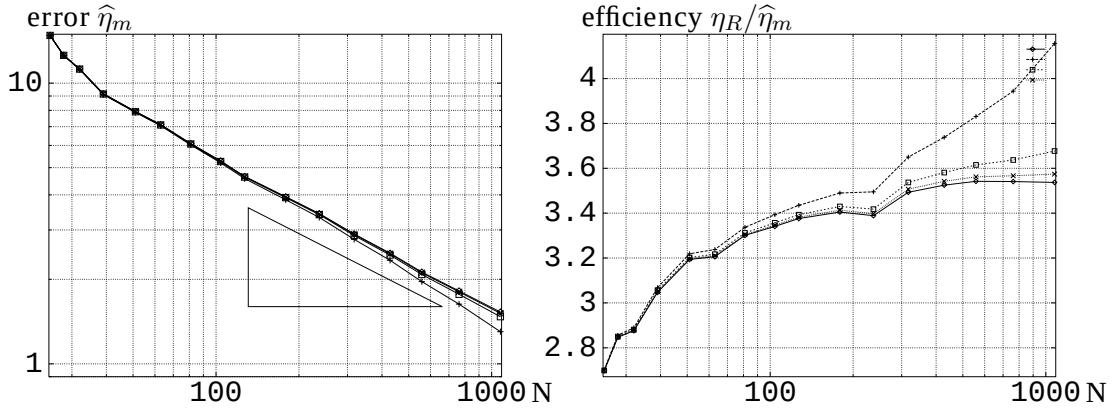

Figure 4.15: a) Reference error $\widehat{\eta}_m$ for $m \in \{\ 1(+),\ 2(\Box),\ 3(\times)\ \}$ compared with reference error obtained from analytical solution $(\diamond)$, little difference for higher refinement levels, triangle has slope -0.5, b) according efficiency indices

calculations we can expect that the efficiency index is overestimated by the ratio $\eta_R/\widehat{\eta}_m$, especially if we observe for higher number of nodes a strong increase of $\eta_R/\widehat{\eta}_m$. We conclude that $\widehat{\eta}_2$ and under some restrictions $\widehat{\eta}_1$ could be used to judge the error estimator.

4.6.2 An example with quasi-monotone diffusion

In a second example we use a more complicated geometry. The diffusion takes on two different values that differ by the factor 1000. We depict the distribution of k in Figure 4.17 by different shadings of the simplices. In the darker part of the domain the diffusion is smaller.

We set constant inflow Neumann boundary conditions on the upper side of the box and Dirichlet boundary conditions on the right side. On the remaining part we impose homogeneous Neumann boundary conditions. Such an example is known as "hydraulic window". We know from theory (see chapter 2) that singularities occur at so called *singular points*, where the interface is not a straight line or where it intersects the boundary. There are at least 10 such singular points. In Figure 4.16 we plot the numerical solution together with the underlying adaptive grid.

Refinement of the grid on the basis of the residual estimator η_R leads to refinement in the neighbourhood of some singular points but other simplices are refined too. This is seen from Figure 4.17, where the adaptive mesh is depicted at different stages of refinement. We observe that the singular points are not refined equally. For instance the singular points on the left side of the boundary are almost not refined. The major refinement happens around the connection of the upper and the lower part of the subdomain with higher diffusion. This part can be seen as a "bottleneck" in a flux problem.

In Figure 4.6.2 a) we draw the reduction of the reference error $\widehat{\eta}_m$ for $m = 1, 2, 3$ and the reduction of the error estimator η_R. We observe an optimal reduction of $\widehat{\eta}_m$ for $m = 1, 2, 3$. But keep in mind that the reference error will be very likely be underestimated for lower values of m.

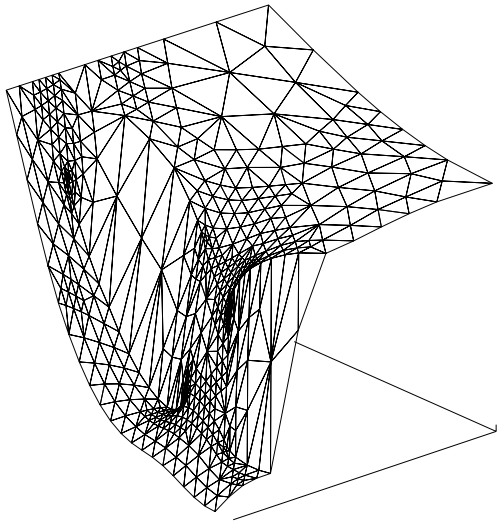

Figure 4.16: Numerical solution and refined grid

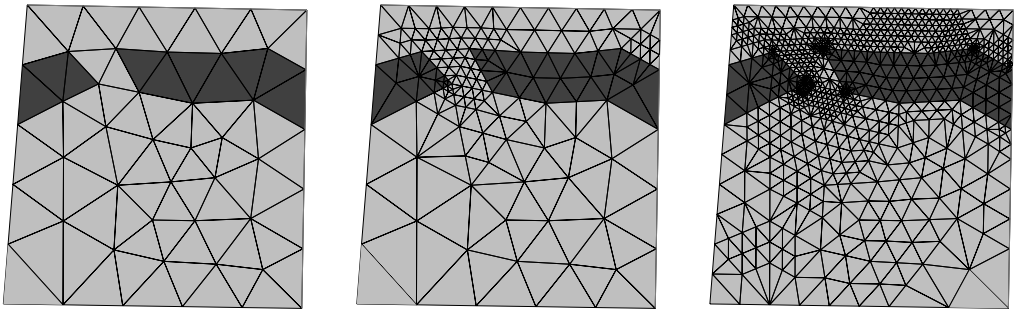

Figure 4.17: Adaptive grid with a) 47 b) 145 c) 843 nodes

The according efficiency indices $\eta_R/\widehat{\eta}_m$ are shown in Figure 4.6.2 b). Again the efficiency index $\eta_R/\widehat{\eta}_m, m = 1,2,3$, is in the range $[2.8, 4.2]$ and increases with the number of unknowns from 2.8 to $3.57, 3.66, 4.2$, depending on $m \in \{1,2,3\}$.
If the singularities were treated by a priori mesh refinement on the basis of the known or approximated degree of the singularity the neighborhood of *all singular points* had have to be refined, regardless of how much the according singular functions actually enter in the solution. The determination of the real contribution of a singular function to the solution would require additional computational effort. This example demonstrates the superiority of the adaptive approach, where no knowledge of the degree of the singularity is needed and where refinement takes place only where needed.

4.6.3 A coal mine

In a third example we use data from the WASY GmbH. The grid discretizes a cut through a mine with small manholes. The ratio of the manhole diameter to the problem

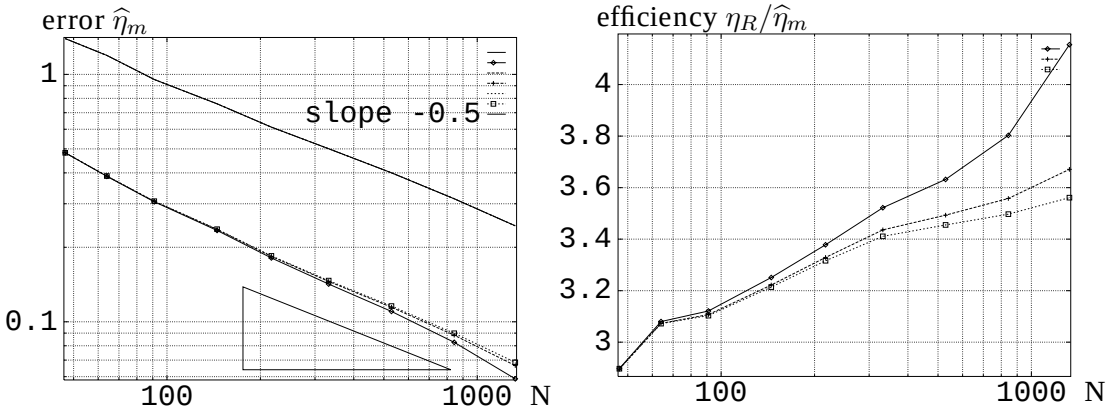

Figure 4.18: a) Reference error $\widehat{\eta}_m$ for $m \in \{\ 1(+),\ 2(\square),\ 3(\times)\ \}$ and η_R (line), triangle has slope -0.5, b) according efficiency indices

size is about $1/500$. We discretize the geometry with about 800 degrees of freedoms. Here triangles with very small or very obtuse angles occur and the ratio of of height versus length of a triangle reaches $1/30$. In Figure 4.19 we plot the diffusion. Inside the manhole (depicted in Figure 4.19 a) by thin black lines) the diffusion is higher by a factor of $1.e5$. We impose Dirichlet boundary conditions at the rightmost manhole in the upper part and inflow Neumann boundary conditions at the leftmost manhole in the upper side of the domain. In the remaining part of the boundary homogeneous Neumann boundary conditions are imposed. Here singularities occur near corners of

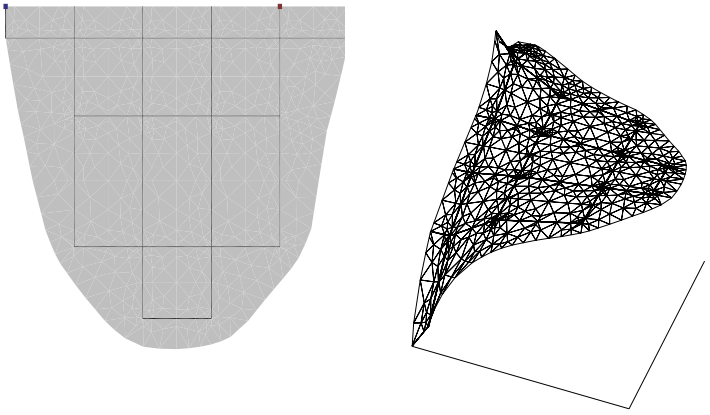

Figure 4.19: a) Domain with higher diffusion coefficient in thin black lines and boundary conditions indicated by small boxes in the upper part b) coarse grid and numerical solution

the manhole. Since the geometry in the neighbourhood of interior singular points is similar the singular solutions will have the same character and regularity. But due to

boundary conditions their contributions to the solution will be likely to be larger in the upper part of the domain and accordingly there they will cause a larger error. This expectation is confirmed by the fact that the gradient of the numerical solution u_h is larger in the upper part as seen in Figure 4.19 b).
In Figure 4.20 we depict the refinement history. We observe that at low refinement stages refinement proceeds near singularities in the upper part of the domain. At later levels refinement occurs also near singularities in the lower part and later near the boundary. This is in agreement with our expectation, that the singularities in the upper part of the domain yield larger contributions to the solution.

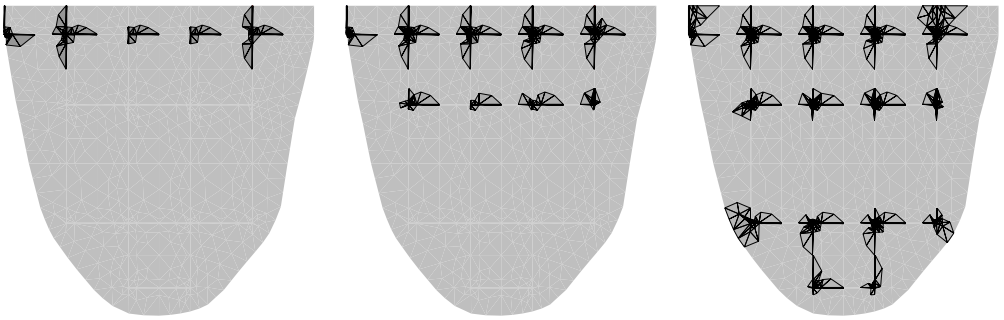

Figure 4.20: Refinement history, we depict simplices which were at least once refined for refinement stages: 5, 11, 25 with 869, 1378, 7161 degrees of freedom; at the beginning, only simplices in the upper part were refined

The estimated error η_R and the reference error $\widehat{\eta}_m$ for $m = 1, 2$ depicted in Figure 4.21 a). We see that $\widehat{\eta}_1, \widehat{\eta}_2$ are reduced again with order slightly better than $O(N^{-1/2})$. We observe that $\widehat{\eta}_1$ has a stronger decay than $\widehat{\eta}_2$ for a larger number of nodes which is due to larger underestimation of the error by $\widehat{\eta}_1$. The estimated error shows the optimal behaviour $O(N^{-1/2})$. Note that this is the case despite the presence of anisotropic simplices. The efficiency index, that is the ratio $\eta_R/\widehat{\eta}_m$, decreases with the number of

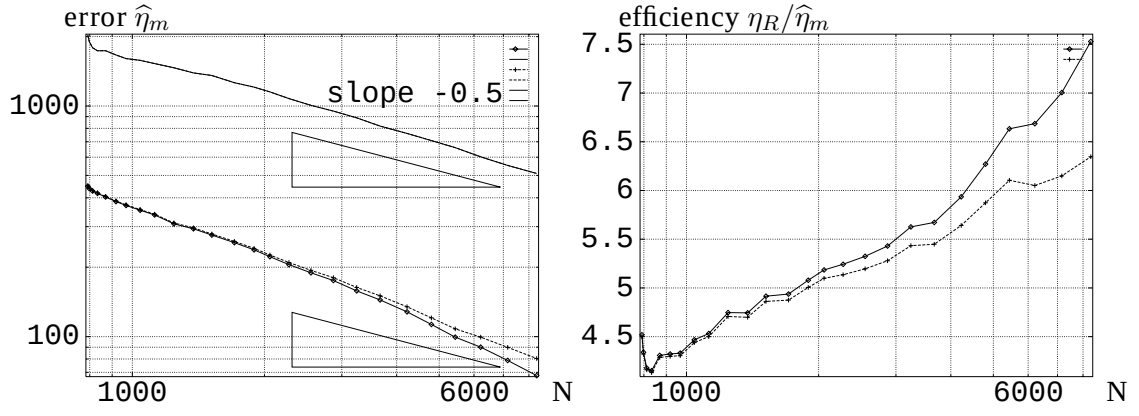

Figure 4.21: a) Estimated error η_R (line) and reference errors $\widehat{\eta}_m$ (line with points) for $m = 1(\diamond), 2(+)$, triangle has slope -0.5, b) efficiency index $\eta_R/\widehat{\eta}_m$ for $m = 1(\diamond), 2(+)$

unknowns only little (by a factor of 2) as depicted in Figure 4.21 b). Remembering that the error is probably underestimated by $\widehat{\eta}_m, m = 1, 2$ we see that the original efficiency index $\eta_R / \ |u - u_h|_{kH^1(\Omega)}$ will be smaller.

4.6.4 An example with heterogeneous data

Again we use data from the WASY GmbH but now the structure of the data is more complicated. The coarse mesh has about 11000 degrees of freedom and the diffusion is fairly heterogeneous, see Figure 4.22. The diffusion varies by a factor of 10. Further we indicate Dirichlet and Cauchy boundary conditions with grey lines.

Figure 4.22: Domain with heterogeneous diffusion and boundary conditions

In Figure 4.23 a) we plot the isolines of the numerical solution. The solution has several local maxima due to interior boundary conditions. The solution of the continuous problem has several hundreds of singularities. As the structure of the diffusion coefficient is complicated, it is not obvious where to expect large errors. In Figure 4.23 b) the refinement depth of the simplices is plotted for the adaptive mesh at refinement level 5. By refinement depth we understand the number of refinements carried out to construct the triangle under consideration. We see that refinement takes place in the vicinity of interior boundaries and near heterogeneities.
The reduction of the estimated error η_R proceeds with order $O(N^{-1/2})$ (Figure 4.24) a). The reduction of $\widehat{\eta}_m$ with $m = 1$ is better but we remember that $\widehat{\eta}_m$ very likely underestimates the error. Note that in the beginning of the refinement the error estimator η_R is reduced with higher order than the asymptotical order. This behaviour is typical for problems with a large number of unknowns and a non-uniformly distributed error.

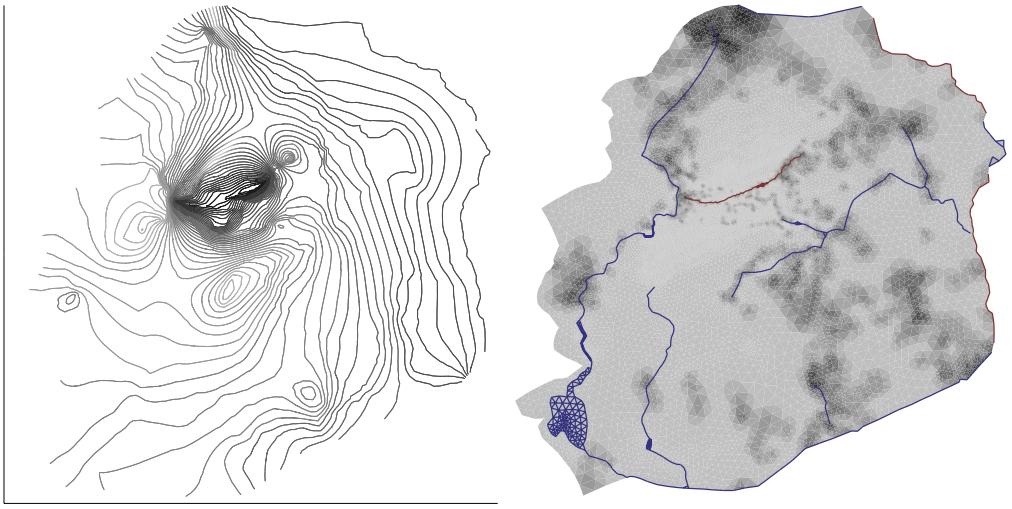

Figure 4.23: a) isolines of numerical solution b) refinement depth of simplices with light grey 0 (not yet refined) to black (5 times refined)

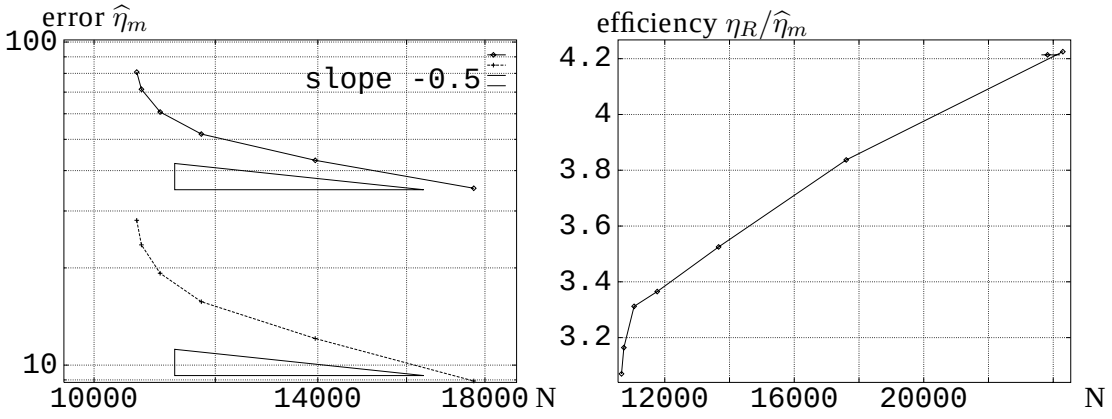

Figure 4.24: a) Estimated error $\eta_R(\diamond)$ and reference error $\widehat{\eta}_m(+)$ for $m = 1$, triangle has slope -0.5, b) efficiency index $\eta_R/\widehat{\eta}_m$ for $m = 1$

In Figure 4.24 b) we draw the efficiency index $\eta_R/\widehat{\eta}_m$. It takes on values between 3 and 4.5. We keep in mind that the error is likly to be underestimated by $\widehat{\eta}_m$.

Note that in the so far presented examples a moderate overestimation of the error occured with more or less *the same problem independent factor in* $[2.7, 6]$. Thus, rescaling the error estimator η_R we obtain an estimator that overestimates the error by a factor at most 2.

4.7 Numerical examples in 3D

In 3D singularities occur along edges and at vertices of the interface (section 2.7). Denote by (r, φ, z) cylindrical coordinates with respect to an edge of the interface. On the other hand it is easy to see that multiplying a 2D singular function $v(r, \varphi)$ with a suitable function $w(z)$ one can construct a 3D-edge singular function.
But if additionally vertex singularities arise, to our knowledge, there is no analytic representation of the singular function, which is piecewise harmonic, available. This is already the case for the Fichera corner (a 3D domain with a reentrant corner of a cube) and the Laplace equation.
Therefore, we decided to compare the error estimator with a reference error that is obtained on the basis of a reference solution calculated on a mesh that is finer than the adaptive one.
In the 2D examples regarded so far, the space spanned by the singular function(s) was 1-dimensional (or at least of finite dimension). In the 3D-problems regarded in [45] [17] 3D edge singularities are 2D singular functions weighted by a function $b(r, z)$ depending on the position z on the edge (see section 2.7.3). The parameter $b(r, z)$ may be very large at some points on the edge and may vanish at other points on the edge. The adapted mesh should then be more refined, where the parameter $b(r, z)$ is large. In subsequent examples we show that firstly, the mesh is refined around singularities and secondly, that it is refined *differently along the edge*.
A-priorily refined grids can not make use of the, in general, unknown function $b(r, z)$ and may provide to an unefficient distributions of nodes along the edge. The following examples will show the superiority of the refinement based on a-posteriori error estimators over a-priori refined meshes.

4.7.1 An example with a box

We define the domain $\Omega := (-1, 1) \times (-1, 1) \times (-1, 1)$ that is divided into $\Omega_1 := (0, 1) \times (0, 1) \times (0, 1)$ and $\Omega_2 := int(\Omega/\Omega_1)$. Set $k_1 = 10000$ and $k_2 = 1$. We impose Dirichlet conditions on the upper and lower side of the box Ω: $u|_{\{1\}\times(-1,1)\times(-1,1)} = 1$ and $u|_{\{-1\}\times(-1,1)\times(-1,1)} = 0$. For the remaining part of the boundary we choose homogeneous Neumann boundary conditions.
We know that singularities arise at edges of Ω_1 which are contained in Ω. Isoplanes of a numerical solution are depicted in Figure 4.25.
Starting with a coarse grid we applied the error estimators $\eta_{R,T}$ to this problem. Isoplanes of the grid size of the adapted mesh are shown in figure 4.26. We see that the mesh is most refined around interior edges of the cube Ω_1. It is less refined away from

these edges. The interior edge of cube Ω_1 parallel to the z-direction is more refined near the vertex $(0,0,0)$ than near the vertex $(0,0,1)$. This is in accordance with the observation that for the point $(0,0,1)$ the contribution of the edge singularity vanishes due to boundary conditions. Thus, we see that the grid is well adapted to the singularities.
A reference solution is calculated on a reference mesh that is obtained by refining globally two times an adaptive grid with approximately 2000 nodes. For comparison of the quality of the reference error other reference solutions were calculated on reference meshes obtained by one time globally refining an adaptive grid and using different parameters θ of the marking strategy. We see in Figure 4.27 a) an optimal decrease of the reference error and the estimated error. There is no dependence on the parameter θ from the marking strategy.
The efficiency indices calculated on the basis of the reference errors increase by a factor at most 2 (Figure 4.27 b)).

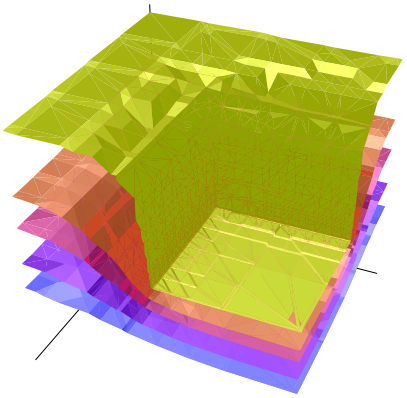

Figure 4.25: Isoplanes of the numerical solution

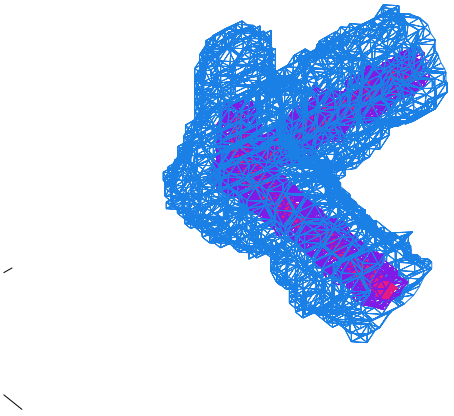

Figure 4.26: Isoplanes of the grid size (wireframe) of an adapted grid (grid is rotated about $90°$ with respect to Figure 4.25)

4.7.2 An example with a more complicated geometry

A more complicated geometry is used in the next example. It consists of a ball and two cylinders. Its triangulation is shown in Figure 4.28. The grid was generated using the grid generator NETGEN from J. Schöberl [54]. Outside the ball the diffusion is higher by a factor 100. We impose constant Dirichlet boundary conditions on the plane faces of the cylinders. For the rest of the boundary we impose homogeneous Neumann boundary conditions.
The numerical solution is depicted in Figure 4.29. Singularities occur around the 1-dimensional spheres S_1, S_2 that are given by the intersection of the surface of the ball with the surface of the cylinders.

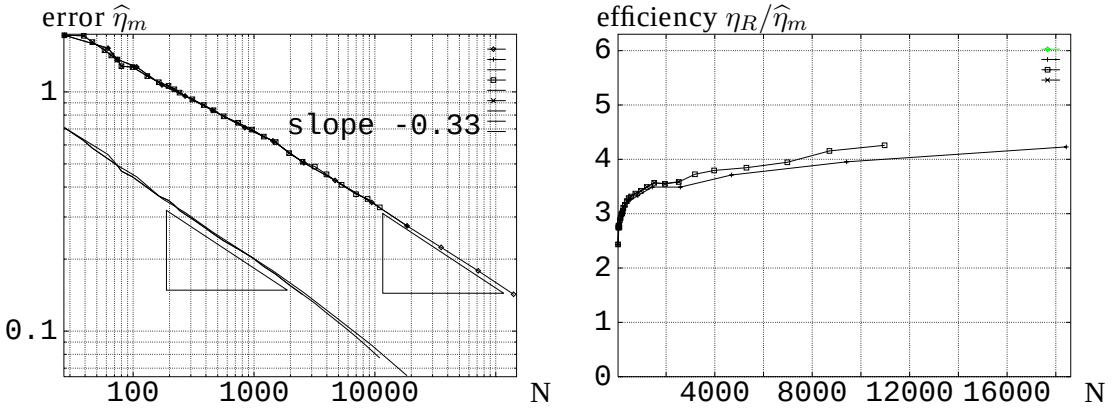

Figure 4.27: a) Reduction of reference errors with order $O(N^{-1/3})$ and for η_R with order near $O(N^{-1/3})$, triangles have slope -1/3, refinement on the basis of estimator η_R, b) efficiency indices are moderately constant

Figure 4.28: Domain consisting of a ball and two cylinders

The numerical solution is depicted in Figure 4.29. As the geometry around the singular edges is similar, the particular singular solutions will have roughly the same regularity. But their contributions to the solution will be different and we expect that their contributions are the larger the larger the gradient. Thus, we expect larger contributions from the singularities where S_1 and S_2 are close together.

A look at some isoplanes of the grid size of the refined grid (Figure 4.30) shows refinement around the spheres S_1, S_2. We see that the grid is indeed more refined on parts where S_1, S_2 that are close together.

The reference errors are reduced with optimal order as shown in picture 4.31 a). The reduction of η_R is a little bit worse but we may expect improvement on more refined grids as the asymptotic stage may not yet been reached.

Comparison of the efficiency index depicted in Figure 4.31 b) shows that the error is overestimated by more or less the same factor as in the example from subsection 4.7.1.

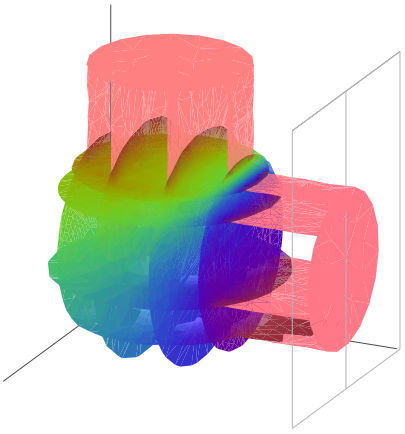

Figure 4.29: Numerical solution

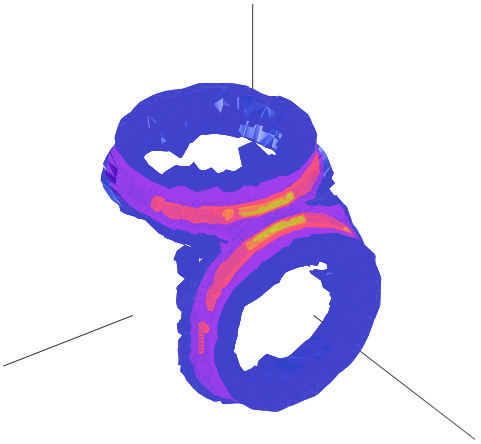

Figure 4.30: Isoplanes of the grid size of an adapted grid

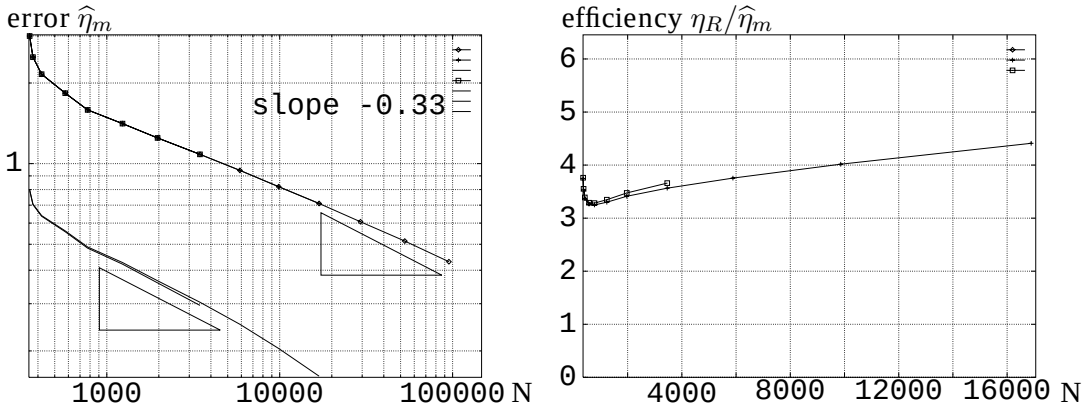

Figure 4.31: a) Reduction of reference errors (lines) with order $O(N^{-1/3})$ and of η_R (line with points) with order near $O(N^{-1/3})$, triangles have slope -1/3, refinement on the basis of estimator η_R, b) efficiency indices are moderately constant

This may indicate, in a certain range, a problem independent efficiency index, as observed in the 2D examples.

4.7.3 Efficiency of isotropic grids for edge singularities

It is known that the edge singularities have an anisotropic nature (see [5] for the Laplace equation): the singular solutions have a strongly varying gradient on lines perpendicular to the edge but in directions parallel to the edge the singular solution is smoother. Isotropic grids make no use of that anisotropy and therefore they may yield a non-optimal relation between the error and the number of nodes. Here anisotropic meshes can pay off [5]. Nevertheless, if the solution has $H^{1+1/3}$-regularity at least there can

be a-priorily constructed isotropic grids which yield an optimal error reduction rate $O(N^{-1/3})$ [6], and we may expect for a-posteriorily adapted grids an optimal error reduction rate too. For a-posteriori error estimators for anisotropic grids see [37] [38] [55].
In order to test the efficiency of adapted isotropic grids applied to edge singularities we pose the following problem. We define a 2D singular solution that will in a second step be extended to a 3D solution. Define the L-shaped domain $\Omega' := (-1,1) \times (-1,1)/([0,1] \times [-1,0])$. Divide Ω by a line into equal parts Ω'_1, Ω'_2, where the diffusion coefficients $k_1 := 1, k_2 > 0$ are given (see Figure 4.32). Set homogeneous Dirichlet boundary conditions on the edge E_D given by the points $(0,0)$ and $(1,0)$. Homogeneous Neumann conditions are imposed on the edge E_N given by $(0,0)$ and $(0,-1)$.
We take a 2D singular solution $v = r^\lambda s_\lambda(\varphi)$ which is piecewise harmonic and satisfies the boundary conditions on E_D, E_N and the interface conditions on $\partial\Omega'_1 \cap \partial\Omega'_2$. Here (r, φ) are polar coordinates and $0 < \lambda < 1$ depends on k_2.

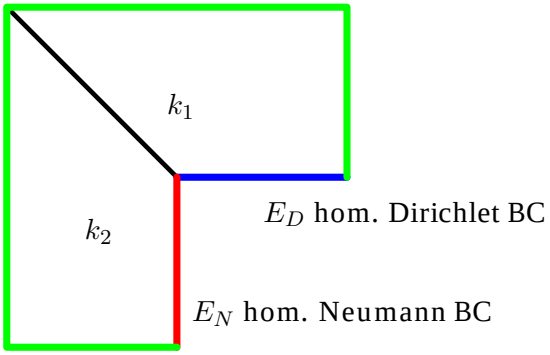

Figure 4.32: 2D domain Ω'

Now we extend the domain Ω' and the function v in $z-$direction. We define $\Omega := \Omega' \times (0,2), \Omega_1 := \Omega'_1 \times (0,2), \Omega_2 := \Omega'_2 \times (0,2)$ and $v_E(r, \varphi, z) := v(r, \varphi)$. Dirichlet boundary conditions are posed according to v_E on $\partial\Omega$ except at $E_N \times (0,2)$ where homogeneous Neumann boundary conditions are set.
Recall that for $k_1 < k_2$ the quasi-monotonicity condition is violated. Calculation shows that in the quasi-monotone case $\lambda \geq 1/3$ and otherwise $0 < \lambda < 1/3$. We know $v_E \in H^{1+\lambda-\varepsilon}(\Omega_i), i = 1,2$, for any $\varepsilon > 0$. There is a $1-1$ relation between k_2 and λ and we will take λ as an parameter.
We use a reference solution which is an approximation of v_E with quadratic elements on grids which we obtained by refining one or two times globally the finest adaptive grid.
As shown in Figure 4.33 the order of reduction of the reference error is optimal for $\lambda = 0.6$. But for $\lambda = 0.2$ the error is reduced with lower order. These results are in accordance with the expectation that on isotropic meshes the error is reduced with optimal order as long the solution has regularity $H^{1+1/3}$. For lower regularity isotropic grids (adapted with the error estimator η_R) are not suited because the reduction of the error may not proceed with optimal order as seen in Figure 4.33.

One may argue that the presented grids are non-optimal in the non-quasi-monotone case and that there are isotropic grids with a smaller error and the same number of nodes. But recall that we have seen in section 4.5 that the estimator may lead to efficient grids also in the non-quasi-monotone case.

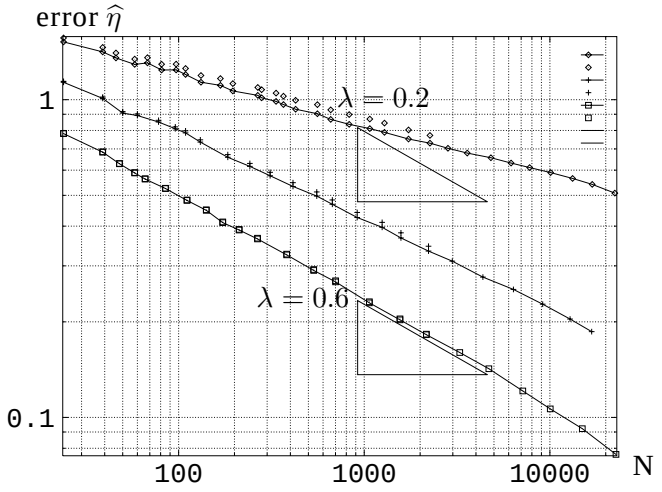

Figure 4.33: Order of reduction of the reference error depends on regularity parameter $\lambda \in \{0.6(\square), 0.4(+), 0.2(\diamond)\}$, triangles have slope -0.33

4.8 Example for a parabolic problem

The following example gives an impression how adapted grids in time look like. We define the domain as in example 2.1 on page 15 with $k_1 = 1, k_2 = 100$ and pose Dirichlet boundary conditions on the left side $g_D(x = 1, y, t) := \max\{1, 1e4 \cdot t\}$, homogeneous Dirichlet conditions on the right side and initial conditions $u(x, y, t = 0) = 0$. On the remaining part of the boundary we pose homogeneous Neumann boundary conditions. The adapted grids were constructed by refining in each time step the coarse initial grid as long as the number of nodes did not exceed 300. The imposed boundary conditions result on an inflow from the Dirichlet boundary. Due to higher conductivity in domain Ω_2 this domain is "saturated" faster and interior boundary layers arise at the interface. As times gets large a singularity at the origin will arise as for the according stationary problem.

In the transient process we differ between an initial, a transient and the stationary stage. During the initial stage for about $0 \leq t \leq 1e3$ the Dirichlet boundary conditions cause a boundary layer. Figure 4.34 a) shows that the boundary layer is resolved on the adapted grid. The singularity at $(0, 0)$ has no large influence on the solution and the grid is not refined there. In the transient stage the boundary layer vanishes and the solution changes much in time on large parts of the domain. This is on our case measured by the entry measuring the difference $u_h^n - u_h^{n+1}$ of the error estimator. In Figure 4.34 b) it

is shown that parts near the interface are stronger refined. There a new inner boundary layer arises due to the higher conductivity in domain Ω_2. At the transient stage the influence of the singularity at the origin grows. The influence of the difference $u_h^n - u_h^{n+1}$ vanishes in the asymptotic stage for approximately $t \geq 10$, where the solution does not differ much from its stationary limit. Now the singularity dominates and we see in Figure 4.34 c) stronger refinement around the origin.

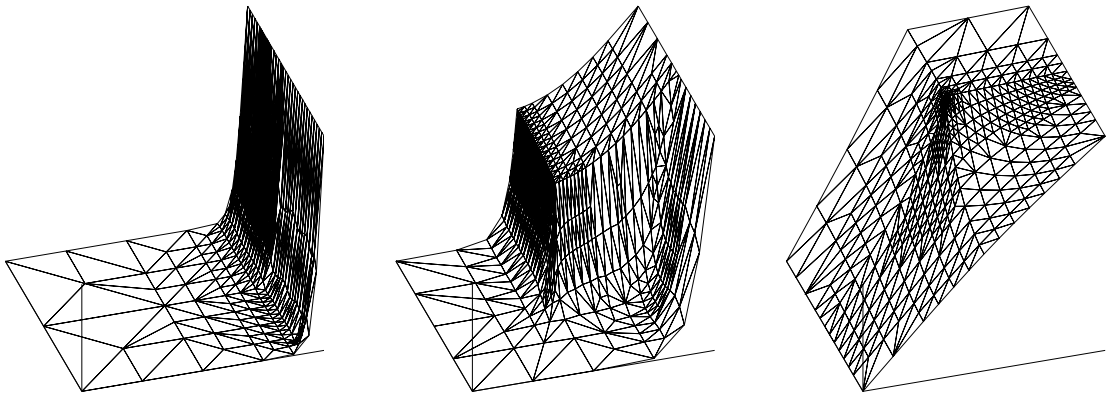

Figure 4.34: Numerical solution at different time levels a) initial stage $t = 3e-3$, b) transient stage $t = 0.7$, c) stationary stage $t = 77$

4.9 Conclusions for the numerical experiments

We have carried out numerical experiments for model problems as well as for problems with real data. For model problems in the quasi-monotone case and for problems with real data the obtained adapted meshes were refined around the singularities and have led to an *optimal reduction of the error* with order $O(N^{-1/2})$. There were no differences concerning the error reduction between the estimators η_R, η_D and η_H. Further the efficiency index has turned out to be moderately constant and *independent of the investigated problems* in the range $[2.5, 5.7]$.

For model problems in the quasi-monotone case we observed an asymptotical value of approximately 3.6. Rescaling by this value one gains error estimators which are near to be asymptotically exact, at least in the range of the regarded model problems. But as the efficiency is in our experiments a monotone increasing function over the number of unknowns the rescaled error estimator will underestimate the error. This is undesired as one would rather prefer the error to be overestimated. The star-based error estimator developed recently in [42] shows a similar behaviour: it seems to be asymptotically exact but it underestimates the error at the preasymptotic stage. In distinction from the problems considered in [42] we neglected the influence of the load function f on the error estimators regarding only problems with vanishing f.

Results obtained in non-quasi-monotone cases indicate dependence of the estimators on the regularity of the problem and the grid. Nevertheless, we observed for sufficiently fine meshes the same asymptotical efficiency index of approximately 3.6 as for quasi-monotone problems and an optimal error reduction rate.
Results obtained in 3D showed an optimal reduction of the error as long as the piecewise regularity is at least $H^{1.5}$.